# Ensemble prediction of coastal flood risk arising from overtopping by linking meteorological, ocean, coastal and surf zone models

RMetS
Royal Meteorological Society

# Ensemble prediction of coastal flood risk arising from overtopping by linking meteorological, ocean, coastal and surf zone models

Qing-Ping Zou,[a]*Yongping Chen,[b,e] Ian Cluckie,[c] Richard Hewston,[c] Shunqi Pan,[d] Zhong Peng[b] and Dominic Reeve[c]

[a]*Department of Civil and Environmental Engineering, University of Maine, Orono, ME, USA*
[b]*School of Marine Science and Engineering, University of Plymouth, UK*
[c]*College of Engineering, Swansea University, UK*
[d]*School of Engineering, Cardiff University, UK*
[e]*State Key Laboratory Hydrology-Water Resources and Hydraulic Engineering, Hohai University, Nanjing, China*

*Correspondence to: Q.-P. Zou, Department of Civil and Environmental Engineering, 577 Boardman Hall, University of Maine, Orono, ME 04469-5711, USA. E-mail: qingping.zou@maine.edu

**This paper presents an integrated 'Clouds-to-Coast' ensemble modelling framework of coastal flood risk due to wave overtopping. The modelling framework consists of four key components: meteorological forecasts, wave–tide–surge predictions, nearshore wave models and surf zone models. This type of ensemble prediction approach allows us to estimate the probabilities of various outcomes and so improve our understanding of the reliability of results. It also provides a measure of the uncertainty associated with predictions, which can be particularly large for extreme storms, and allows us to assess how the uncertainty propagates from meteorological forecasts to overtopping and subsequent coastal flood risk predictions. Copyright © 2013 Royal Meteorological Society**

*Key Words:* coastal flooding; overtopping; extreme events; ensemble prediction; uncertainty; sea wall

*Received 16 November 2011; Revised 7 October 2012; Accepted 16 October 2012; Published online in Wiley Online Library*

*Citation:* Q-P Zou, Y Chen, I Cluckie, R Hewston, S Pan, Z Peng and D Reeve. 2013. Ensemble prediction of coastal flood risk arising from overtopping by linking meteorological, ocean, coastal and surf zone models. *Q. J. R. Meteorol. Soc.* DOI:10.1002/qj.2078

## 1. Introduction

Recent UK government reports (OST, 2004; DEFRA, 2005) have shown that the UK's assets at risk from flooding by the sea are valued at £132.2 billion and from coastal erosion at £7.8 billion, and some 4 million people and properties in England and Wales alone are under threat. These values are expected to grow significantly in the future as projected changes in climate lead to further sea-level rise and increasing storm frequency and severity. The protection of coastal communities and the effective government planning of capital expenditure both rely on our ability to predict the impact of storms on sea defences.

The UK coastal flood defences are usually designed to withstand storm events with a return period of between 50 and 200 years, taking account of sea-level rise. Such events are termed 'design events'. A design event could simply be a given wave height or high water level. In coastal and estuarine areas, the design event will usually be a combination of many variables, including wave conditions (height, period and direction), wave and wind set-ups, tides, storm surge, river flows and foreshore height. The design event is an important concept because it simultaneously defines the level of protection that is going to be provided by a defence while also acknowledging that the structure will not provide absolute protection under all conditions. Two important derived variables are: the water depth – the difference between the still-water level and foreshore level; and the freeboard – the difference between the crest level of the structure and the still-water level. The water depth provides some control on the height of waves that can reach

the structure without breaking, while the freeboard is a major factor in determining the volume of wave overtopping.

Flooding occurs when there is a failure of a defence. This can arise from a functional failure (the conditions exceed those for which the defence was designed) or a structural failure (where some element or components of the defence do not perform as intended under the design conditions). The former arises from society's need to find a compromise between the cost of the defence and the consequences of a flood, and the latter is generally more dangerous as they are unexpected, and have been the source of recent notable flooding events. Two major causes of structural failure are: low freeboard leading to excessive wave overtopping of the defence, then leading to erosion of the back and crest of the defence, or even damage to the armour layers; and toe failure, where erosion of the foreshore at the base of the defence occurs to such an extent that the structure is undermined and collapses (see CIRIA, 1986).

The design of coastal defences and the assessment of their performance often rely on a qualitative review of water depth changes in front of the sea defence. An increase in water depth at a structure for a fixed tide level would enable larger waves to reach the structure before breaking. Tidal level and storm surge are both important in determining water depth and depth-limited wave breaking in front of the structure. Wave set-up serves to amplify this effect. How the uncertainties in wave conditions are modified through propagation to the shore, their interactions with surge, tide, sediment movements and subsequent beach profile changes are critical to determining whether a defence will be sufficient or overwhelmed with subsequent flooding and damage.

The objective of the work presented here is to develop a framework, based on tested computer models, through which the inherent uncertainties can be better quantified. A key aim of the project is to integrate meteorological models, regional hydrodynamic (waves, tides and surge) models and surf zone hydrodynamic models to construct an ensemble prediction framework of coastal flood risk. In contrast to earlier studies of coastal flood risk (Reeve and Burgess, 1993; Meadowcroft *et al.*, 1996; Reeve, 1998), this approach not only provides a quantitative measure of the uncertainty associated with predictions, which can be particularly large for extreme storms, but also, with use of ensemble techniques, allows us to estimate the probabilities of different outcomes. Furthermore, it is also possible to assess how the uncertainty propagates from meteorological forecasts to overtopping and coastal flood risk, thereby improving our understanding of the reliability of results (Zou and Reeve, 2009; Dance and Zou, 2010). The ensemble modelling approach has been used widely in meteorology and storm surge studies (Horsburgh *et al.*, 2008; Flowerdew *et al.*, 2010), but less so in coastal engineering.

This study uses a major storm event that occurred between 25 and 30 October 2004 as a test case to illustrate the proposed approach. This storm was widely reported to have caused severe damage to coastal defences along the southwest coast of the UK (Magar *et al.*, 2009). During the storm, high wave and surge heights were recorded in the English Channel, and several cases of overtopping of sea defences and damage to sea walls were observed (see Figure 1). Examples include the flooding at Newlyn and Portmellon and overtopping occurred along part of the sea wall between Dawlish and Teignmouth, which protects the mainline railway. The Newlyn site was specifically selected for the application of the present ensemble prediction framework because of the observed overtopping and damage and availability of wave and tide observations nearby. For this particular storm event, the wave heights themselves in Newlyn Harbour were not exceptional for equinoctial storms but what made this storm particularly unusual were the wave direction and high water levels accompanied by high waves.

(a)

(b)

**Figure 1.** (a) Storm-induced wave overtopping at Portmellon, Cornwall (Photograph by Marie Preece). (b) Storm damage to the sea wall protecting the mainline railway between Dawlish and Teignmouth. © Network Rail. This figure is available in colour online at wileyonlinelibrary.com/journal/qj

## 2. Methodology

To achieve the objectives of the study, the ensemble modelling framework includes four interlinked strands: (i) meteorological modelling to downscale global model forecasts; (ii) regional hydrodynamic modelling of waves, tides and surge; (iii) nearshore wave modelling; and (iv) surf zone model, as shown in Figure 2.

### *2.1. Meteorological models*

Meteorological models routinely run over the UK domain in national weather centres usually have such a coarse spatial and temporal resolution that their output is insufficient to drive models of surge and wave generation and propagation at the regional scale. The regional hydrodynamic models

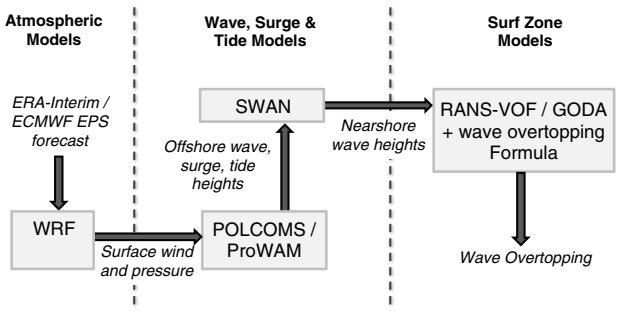


**Figure 2.** Integrated 'Cloud to Coast' ensemble modelling framework for coastal flood risk arising from overtopping and scour.

require input of atmospheric pressure and wind field at each node at each time step, and therefore a downscaling procedure is required to bridge the scale gap between the large-scale meteorological modelling domains and the regional and coastal modelling domains. Given the dynamic nature of extratropical cyclones, which are of interest in this study, simple linear interpolation of the atmospheric pressure and wind field can produce unrealistic results (Winter *et al.*, 2008). Other methodologies for downscaling in this environment range from simple statistical methods (Pryor *et al.*, 2005), to high-resolution climate model techniques, (Weisse *et al.*, 2005). Although computationally more expensive, dynamical downscaling is preferable when the features of interest are extreme extratropical cyclones (Pryor *et al.*, 2005; Schwierz *et al.*, 2010).

In this study, the Weather Research and Forecasting (WRF) modelling system is used to resolve the dynamics over high-resolution grids. The WRF model is a next-generation mesoscale numerical weather prediction and data assimilation system, and is thoroughly detailed by Skamarock *et al.*(2008). For this study the ARW (Advance Research WRF) dynamical core of WRF version 3.1 is used to dynamically downscale coarse meteorological data, and generate high-resolution wind and pressure fields as input for the hydrodynamic models.

### 2.2. *Wave, tide and surge models*

To transform the meteorological information to the oceanic and coastal hydrodynamic conditions (waves, tides and surge), which are subsequently used to drive the wave and current model in the surf zone, a third-generation spectral wave model (ProWAM) and a 3D baroclinic tide and surge model (POLCOMS) with full two-way coupling are used. The ProWAM model, a revised version of WAM model, solves a wave action balance equation without any predefined shape of the energy spectrum and predicts the wind and swell wave fields from surface forcing and other oceanic processes (see Günther *et al.*, 1992; Monbaliu *et al.*, 2000). The POLCOMS model was developed at Proudman Oceanographic Laboratory (presently National Oceanography Centre, Liverpool). The model solves equations of state and motion, and includes surface forcing, river discharges and turbulence closure. The model is capable of computing three-dimensional flow, turbulence, salinity and other hydrodynamic parameters at oceanic and coastal scales, see Holt and James (2001), Wolf *et al.*(2002), Osuna *et al.*(2004) and Pan *et al.*(2009) for further details. In the present study, the POLCOMS model is used for computing the tides, tidal currents and surge, while waves are computed by the fully coupled ProWAM model.

### 2.3. *Nearshore wave model*

To further refine the wave field produced by the POLCOMS/ProWAM models at relatively coarse resolution (about 3–5 km), the SWAN model is nested to provide higher-resolution hydrodynamics close to the surf zone. Output from the SWAN is then used to define the wave condition at the seaward edge of the surf zone, which is the input to the surf zone model.

The SWAN model is a third-generation spectral wave model that computes random, short-crested wind-generated waves in coastal regions and inland water, based on wind, bottom topography, currents and tides (Booij *et al.*, 1999). The SWAN model accounts for wave triad and quartet interactions, depth-induced wave breaking, bottom friction and whitecapping dissipation. It is therefore particularly suitable for calculating the nearshore wave transformation from deep to shallow water at Newlyn Harbour.

### 2.4. *Surf zone models*

At the finest resolution, the Reynolds-averaged Navier–Stokes volume of fluid (RANS-VOF) model, originally developed by Lin and Liu (1998), is used to predict the wave overtopping discharges. The RANS-VOF model solves the 2D Reynolds-averaged Navier–Stokes equations by decomposing the instantaneous velocity and pressure fields into the mean and turbulent components. Reynolds stresses were described by an algebraic nonlinear $k$–$\varepsilon$ turbulence model. A volume of fluid (VOF) method developed by Hirt and Nichols (1981) was used to capture free surface flows. More detailed information about the model and its implementation for overtopping predictions can be found in Lin and Liu (1998) and Peng and Zou (2011). Recently this model has been further developed and used widely to investigate wave–structure interactions (Garcia *et al.*, 2004; Lara *et al.*, 2006; Peng and Zou, 2011; Zou and Peng, 2011), where extensive formal convergence and stability tests of the model were conducted. This model was also used to simulate wave overtopping over rubble mound breakwaters by Losada *et al.*(2008) and over a smooth impermeable sea wall by Reeve *et al.*(2008). Shao *et al.*(2006) found that both RANS-VOF and SPH models produced much better overtopping predictions than the conventional nonlinear shallow-water (NLSW) model over an impermeable sea wall and that the former slightly outperforms the latter.

### 2.5. *Model integration*

The meteorological models, regional hydrodynamic models for waves, tides and surge, nearshore and surf zone models described in the previous sections are linked and applied to the given scenarios. In operation, the downscaled wind and pressure fields from the meteorological model are used to drive the wave, tide and surge and nearshore wave models. The predicted wave conditions and mean water levels at the offshore boundary of the surf zone are in turn used to drive the surf zone model to predict the overtopping at the sea wall and associated coastal flood risk. In the following section the set-up and testing of the individual models are discussed in more detail.

To assess the uncertainties from different components of the modelling system and understanding the propagation of the uncertainties within the modelling system, an ensemble approach is used. Briefly, an ensemble of 50 realizations is generated with the meteorological models. Each of these realizations is then used to drive the wave, tide and surge model, which in turn is used to provide the boundary conditions for the surf zone model. In this manner, a set of 50 possible outcomes (the ensemble) of meteorological conditions is created, together with their corresponding wave and surge conditions and the transformation of these conditions to the sea wall at Newlyn. The uncertainties in flood predictions due to overtopping can be quantified from this ensemble. Statistical analysis of the ensemble also provides an estimate of the propagation of uncertainty from the meteorology model to the wave, tide and surge model and to the surf zone model (Zou and Reeve, 2009).

## 3. Model set-up

The modelling system was set up over the eastern Atlantic Ocean with progressively finer nested domains centred at Newlyn for the storm event that occurred between 25 and 30 October 2004.

### 3.1. *Meteorological modelling*

In order to accurately simulate surface wind speeds, the meteorological model must be run at a sufficiently high temporal and spatial resolution to capture the transfer of energy to the lower atmospheric levels. The WRF model is run at a 27 km spatial resolution with a time step of 60 s, over a domain spanning 22°W to 12°E and from 42°N to 67°N (Figure 3). In addition, four-dimensional data assimilation is employed whereby WRF is run with extra nudging terms enabling the simulation to be kept on track with the driving data, while maintaining its dynamical consistency. This is achieved through point-by-point nudging of horizontal winds, temperature and water vapour variables in the driving data to a 3D space- and time-interpolated analysis. After undertaking a suite of sensitivity tests it was found that the added value of a three-nested WRF model configuration, with spatial resolutions of 27 km, 9 km and 3 km, did not provide a significant increase in the reliability of surface wind speed and surface pressure values over the open ocean. While significant improvements were seen over land, the fact that the hydrodynamic model utilizes model output from over the open ocean, and given the computational expense of the three-nest configuration, a single-nest approach was taken.

For the validation period (1 October to 7 November 2004) the ECMWF (European Centre for Medium-range Weather Forecasts) reanalysis dataset ERA-Interim is used to initialize the model and define the lateral boundary conditions. In addition, for the period 26 October to 3 November data from the ECMWF Ensemble Prediction System (EPS) are used. The EPS is comprised of one deterministic forecast and 50 physically perturbed forecasts. Each member of the ensemble is initialized with slightly different atmospheric conditions, and each is generated using different parametrizations of subgrid-scale physical processes (a more detailed description of the EPS is provided by Persson and Grazzini, 2007). Each individual ensemble member merely represents the possible track and intensity that depict the variability in the evolution and dissipation of an extra-tropical cyclone (a nonlinear chaotic system), with each having a very small likelihood of occurrence. At the time of the storm (October 2004) the operational ECMWF model was integrated at the TL255 spectral resolution (approximately 80 km horizontal resolution), with 40 vertical layers.

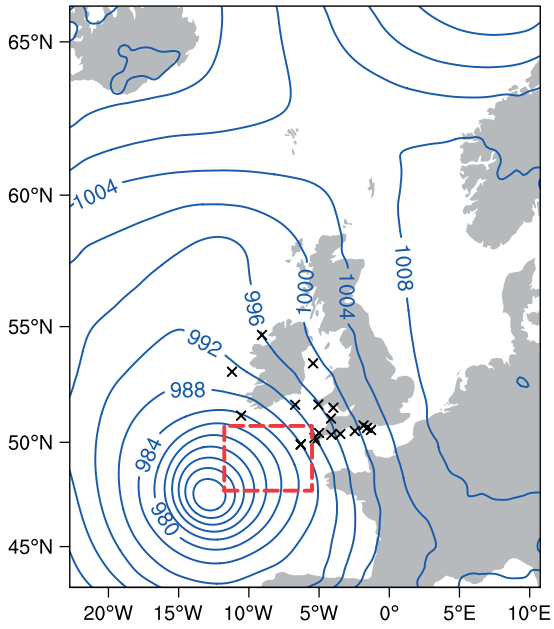


**Figure 3.** Sea-level pressure (mb) at 0600 UTC 27 October 2004 from downscaled ERA-Interim data. Crosses identify surface stations used in the verification process. Results from a limited area domain (dashed box) are discussed in section 5.1. This figure is available in colour online at wileyonlinelibrary.com/journal/qj

The main physical parametrizations within WRF include the WRF single-moment 3-class microphysics scheme (Hong *et al.*, 2004); rapid radiative transfer model (RRTM) for long-wave radiation (Mlawer *et al.*, 1997); Dudhia short-wave radiation scheme (Dudhia, 1989); Yonsei University planetary boundary layer scheme (Hong *et al.*, 2006); and the Kain–Fritsch cumulus parametrization scheme (Kain, 2004). In addition, the Noah land surface model (Chen and Dudhia, 2001), with four layers of soil temperature and moisture, was used.

### 3.2. *Wave, tide and surge models*

The modelling system for waves, tides and surge consists of two cascading domains: the large/coarse grid domain, covering the northeast Atlantic Ocean from 20°W to10°E and from 45°N to 65°N, and the downscaled fine-grid domain covering the English and Bristol Channels from 8.0°W to 4.5°E and from 48.0°N to 52.5°N, as shown in Figure 4. The resolutions for the coarse- and fine-grid domains are 1/10° × 1/10° and 1/20° × 1/20° respectively. The model is run on the coarse-grid domain first, forced by the wind field and sea-surface pressure obtained from the meteorological model. The model is run again over the fine-grid domain, forced by the wave conditions along its open boundaries from the model results over the coarse-grid domain, and also the tides from the tide model CS3 (Flather and Williams, 2004; Williams and Flather, 2004).

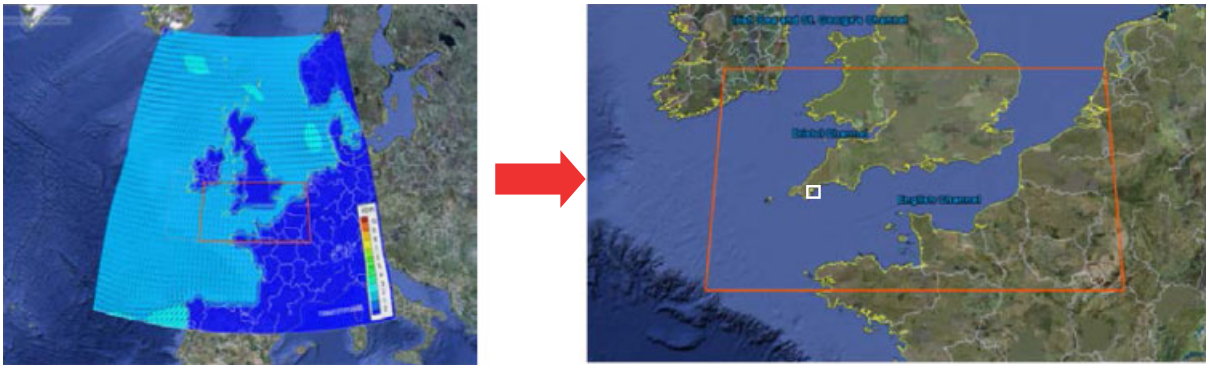

**Figure 4.** Schematic diagram of three-tier nested computational domains for wave, tide and surge modelling. The smallest domain indicated by the white box is for the nearshore wave model SWAN (see Figure 5 for an enlarged view). This figure is available in colour online at wileyonlinelibrary.com/journal/qj

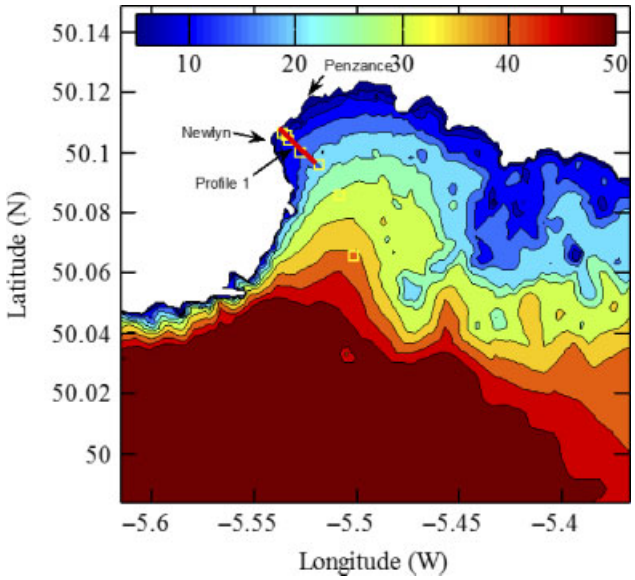


**Figure 5.** Computational domain and the bathymetry for SWAN (denoted as white box in Figure 4). Squares stand for the output locations of the SWAN model; Thick straight lines over the squares represents the cross-section over which the surf zone model is implemented. This figure is available in colour online at wileyonlinelibrary.com/journal/qj

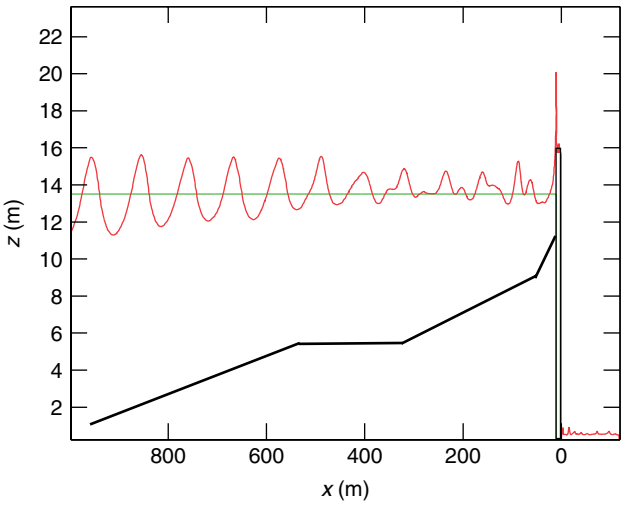


**Figure 6.** RANS-VOF surf zone model set-up. The wavy and horizontal straight lines denote the surface elevation and the still-water level. Thick black lines indicates the beach profile. The sea-wall is located at $x = 0$. This figure is available in colour online at wileyonlinelibrary.com/journal/qj

### 3.3. *Nearshore wave model*

As described earlier, the third-generation nearshore wave model, SWAN, is used to generate the wave conditions at the offshore edge of the surf zone with which to drive the surf zone model. Figure 5 shows the computational domain and the bathymetric data for SWAN wave modelling. Wave conditions and water depth output at a water depth of 50 m from the POLCOMS and ProWAM models were applied at the offshore boundary to drive the SWAN model. The bathymetry data were obtained from the Seazone database (Digimap), with a resolution of 1/10 arcmin (about 137 m × 184 m at a latitude of 50°N). The tide level/water depth used by SWAN varies with time. Land points (recognized initially with bathymetry data) are excluded from the computations and the computational domain has a resolution of 70 m × 90 m.

### 3.4. *Surf zone model*

The SWAN model cannot properly simulate the wave overtopping at the sea wall. It is evident from Figure 5 that depth contours are parallel so that, to a first approximation, alongshore variation can be ignored in front of the sea wall at Newlyn. In addition, due to refraction, wave crests become parallel to the bottom contour and coastline at the sea wall. Therefore, the wave transformation at the site can be well captured by a 2D vertical (2DV) surf zone hydrodynamics model.

Wave transformation across the surf zone is performed using the RANS-VOF model. This is a 2D (vertical slice) model and is applied along a cross-shore transect in the $x$-axis direction that meets the land at Newlyn where damage occurred to the seawall (Magar *et al.*, 2009). The transect is indicated by the straight line over the squares in Figure 5. A schematic diagram of the computational domain and geometry at the Newlyn sea wall is shown in Figure 6 and is 1120 m × 24 m. The seaward boundary of the model is at $x = 1000$ m and the rear edge of the vertical wall is located at $x = 0$ m. The seabed profile has been composed from bathymetric measurements gathered from several sources and at different resolutions ranging from 120 m in the seaward zone to 5 m near the coast. Offshore wave conditions are generated at $x = 1000$ m based on the wave characteristics produced by the SWAN wave model. There are 1044 cells in the horizontal direction and 68 in the vertical direction. The cell size varies in the $z$-direction from

0.5 m near the sea bed to 0.25 m around the free surface. The cell size in the $x$-direction ranges from 0.5 m to 2.5 m. The front face of the sea wall is concrete and hence considered to be impermeable. For numerical modelling purposes, the surface of the sea wall is also assumed to be hydraulically smooth, which will provide a conservative (i.e. worst-case) estimate of overtopping. The water depth at the toe of the structure is calculated from the sum of the mean water level and the tidal level minus the sea-bed level. Wave conditions are assumed to be constant during each hour and normally incident against the vertical wall.

Ideally overtopping should be determined from a long sequence of random waves with the appropriate statistical properties. In this paper, the offshore wave–tide–surge model gives integrated wave quantities ($H_s$, $T_z$) and so sequences of random waves would have to be generated that matched these integrated quantities – in a manner similar to that in McCabe *et al.*(2011). While it seems reasonable to expect overtopping by random waves to be largely due to the higher waves, reported observations of wave-by-wave overtopping are extremely scarce (Hunt-Raby *et al.*, 2011). The studies that have been published are not entirely supportive of this expectation. For instance, Tsuruta and Goda (1968) generated regular and irregular waves and measured mean rates and individual volumes of overtopping at a vertical wall. They report that the mean overtopping rates of irregular waves were always smaller than those of equivalent-sized regular waves, but the difference reduced as the wave height decreased. They also compared estimates of the overtopping volumes from irregular waves against the volumes determined for regular waves, finding good agreement for waves of the same crest height, albeit with considerable scatter.

Instead, we have used an approach that is in alignment with current engineering guidance. For instance, the Rock Manual (CIRIA & CUR, 1991) states the following:

> If extreme run-up levels exceed the crest level the structure will overtop. This may occur for relatively few waves under the design event, and a low overtopping rate may often be accepted without severe consequences for the structure or the area protected by it. Sea walls and breakwaters are often designed on the basis that some (small) overtopping discharge is to be expected under extreme wave conditions. The main design problem therefore reduces to one of dimensioning the cross-section geometry such that the mean overtopping discharge, Q, under design conditions remains below acceptable limits.

'Design conditions' are usually storm conditions and specified in terms of a particular value or values of Hs, Tz and water level. Mean overtopping discharges are determined on the basis of empirically derived formulae involving the quantities $H_s$, $T_z$ and water level. Current engineering practice is based on using a regular wave approach that makes appropriate allowances that there will be some waves with $H > H_s$ during a storm. Additionally, it should be noted that in the case we consider wave breaking is clearly an important limiting factor on the height of the waves that can reach the sea wall (as illustrated in Figure 6). This means that the largest waves are partially dissipated by breaking before the structure, and the Rock Manual approach will give a conservative estimate of the overtopping in these cases.

## 4. Model validation

### 4.1. Meteorological modelling

First, the results from the meteorological model must be verified. In this section we present results comparing hourly values of surface wind speed and mean sea-level pressure derived from the ERA Interim reanalysis (ERA-I) and the dynamically downscaled ERA Interim product (WRF-ERA), with observations from a number of locations around the British Isles.

Hourly surface wind speed and mean sea-level pressure observations from the network of UK Met Office stations (UK Met Office, 2010) are used, as well as Irish Marine Institute (2010) buoy values. The locations of these stations are shown in Figure 3. The raw reanalysis data (ERA-I) are linearly interpolated from a 6-hourly resolution to produce hourly values. The period of verification spans from 15 October to 6 November 2004.

Wind speeds derived from the downscaled reanalysis data (WRF-ERA) are shown to be more reliable at capturing the variance of observed wind speeds than ERA-I data (correlation coefficients of 0.92 and 0.90 respectively). Further, ERA-I has a markedly higher bias ($+0.51$ m s$^{-1}$) compared to ERA-WRF (0.40 m s$^{-1}$). If just the storm period is considered (24 October to 2 November 2004) WRF-ERA has a correlation coefficient of 0.87, and exhibits a positive bias of 0.04 m s$^{-1}$. Corresponding values for ERA-I are 0.83 and 1.59 m s$^{-1}$. These values suggest that WRF significantly reduces the absolute error and is more able to fully capture the wind speed variability, particular during the storm period.

The Taylor diagrams (Figure 7) provide information on the correlation between the model wind speeds and observations, while simultaneously showing differences in the variances. Normalized standard deviation values exceeding 1 indicate that model values have a greater standard deviation compared with observed values. Both plots suggest that a greater correlation is shown between the WRF-ERA wind speeds and the observations (dots), compared to the ERA-I values and observations (crosses). In addition, the variance of the WRF-ERA dataset is a lot closer to that of the observed, compared to ERA-I.

Hourly mean sea-level pressure from ERA-I and WRF-ERA is also compared with observations. While the ERA-I and WRF-ERA both correlate extremely well with the observations (both have correlation coefficients exceeding 0.99), the storm period ERA-I features a negative bias of $-0.47$ hPa, while WRF-ERA displays a positive bias with half the magnitude (0.22 hPa).

In summary, we consider that good results have been achieved with the WRF model, and that more reliable wind and pressure fields have been generated than would have been obtained by using the coarse-resolution reanalysis data. In addition, the output fields are of a temporal and spatial scale suitable for input into the regional hydrodynamic models.

### 4.2. Wave, tide and surge modelling

The results of the wave, tide and surge models (POL-COMS/ProWAM) were verified against the measurements obtained from selected tide/surge gauges and wave buoys

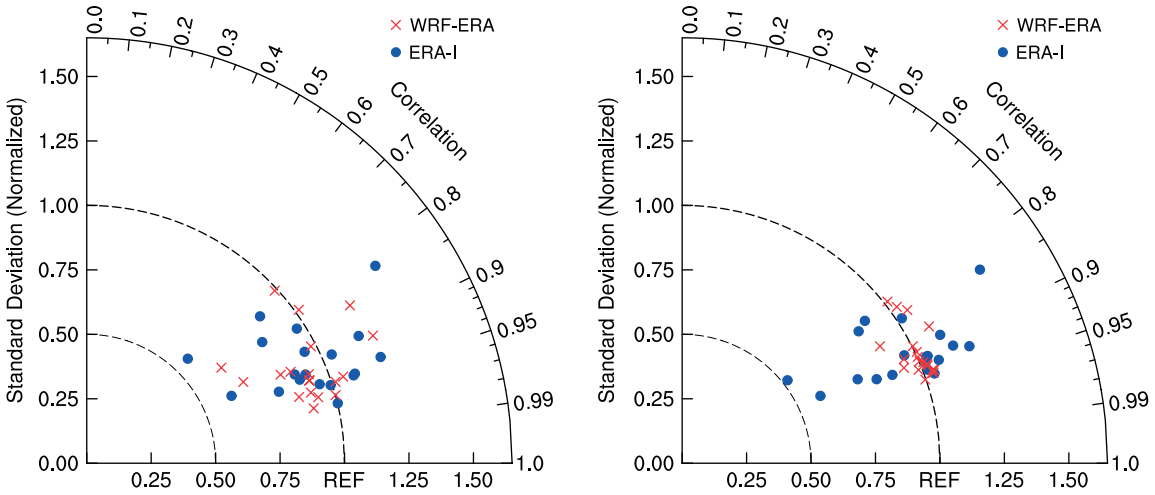


**Figure 7.** Taylor diagrams for WRF-ERA (crosses) and ERA-I (dots) wind speed values at the 19 observing stations shown in Figure 3, for 15 October to 3 November 2004 (left) and 26 October to 2 November 2004 (right). The radial axis indicates the correlation of the model wind speed with observations at each station. Normalized standard deviation is a measure of the standard deviation of the model values compared with the standard deviation of the observed values, at each station. This figure is available in colour online at wileyonlinelibrary.com/journal/qj

in the English Channel (see Figure 8). For verification purposes, the model was run using the ocean surface forcing of wind and atmospheric pressure fields provided by the downscaled reanalysis data (WRF-ERA), also referred to as the control condition. The measurement data were provided by the British Oceanographic Data Centre (BODC: http://www.bodc.ac.uk).

Predicted wave heights, water and surge levels at locations corresponding to the measurement stations are extracted for the comparisons. Figure 9 shows the computed tidal and surge levels at the Newlyn site, which is indicated in Figure 8, and clearly indicating a good agreement with the measurements. The comparisons clearly show a good agreement for tides, and in general for surge at this station, but with up to 0.15 m over-prediction during the storm peak. The surge levels were calculated by subtracting the tide levels representing the tide-only benchmark case from the total water level for the storm event. Therefore, any mismatch in tidal phase may have considerable effect on surge level. Comparisons at other stations (not shown here) also indicate that the model and model parameters have been set up properly to yield satisfactory results. Flather (1984) demonstrates that predicting surge to within 15 cm is regarded as good.

Figure 10 shows the computed significant wave heights ($H_s$) from the control conditions plotted with the measurements at Boscombe and Folkstone, located midway and at the eastern end of the English Channel respectively. In general, the wave heights are computed reasonably well, except at the peak of the storm (27–28 October 2004), where the computed wave heights are smaller than the measurements (by up to 0.5 m at Boscombe, for example). These slight disagreements may reflect the inability of the WRF-ERA data to fully capture the temporal and spatial variability in the wind and pressure fields during the storm.

### 4.3. *Surf zone modelling*

Wave overtopping discharge is equal to the volume flux at the crest of structure; therefore, Schüttrumpf and Oumeraci (2005) proposed that the overtopping discharge can be calculated from the product of the layer thickness and velocity at the crest. The formulae for calculating overtopping discharge can be found in Schüttrumpf and Oumeraci (2005) and Peng and Zou (2011). We found that both the layer thickness and velocity at the crest display large variations with time even for constant wave height and water depth, consequently leading to large variations of wave run-up and overtopping. This behaviour may be attributed to the randomness associated with nonlinearity, wave breaking, turbulence generation and dissipation.

The predicted overtopping discharge over sloping and vertical seawalls is validated by the empirical formulae of TAW (2002) and Van der Meer and Janssen (1995) in Figure 11. Computed overtopping discharges are in good agreement with both formulae for relative freeboard between 0.2 and 1.4. The overtopping discharge is underestimated for relative freeboards larger than 1.2 because the present model fails to capture the overtopping volumes of small splashes and neglects the entrained air effect (Peng and Zou, 2011).

The diamonds in Figure 11 represent the overtopping predictions by the RANS-VOF model over the sea wall in Newlyn. For each of 50 ensemble members, RANS-VOF model simulations were performed at high tide during the peak of the storm at 1700 UTC 27 October. The blue straight solid line denotes the wave overtopping predictions by the empirical Eq. 7.3 in EurOtop (2008). Wave overtopping over a vertical wall calculated by the RANS-VOF model is also in general agreement with that of the empirical Eq. 7.3 in EurOtop (2008). The large scatter in RANS-VOF model predictions is due to the uncertainty and random nature in overtopping events as well as model errors. The dimensional overtopping $q$ for the blue diamonds shown in Figure 17 (bottom panel) generally exceeds 0.05 $m^3\ m^{-1}\ s^{-1}$, which is the damage threshold for revetment sea walls. This is in agreement with the observed overtopping and damage at the site.

Figure 11 also indicates that the accuracy of model prediction is slightly improved compared to Reeve *et al.*'s (2008) RANS-VOF model results. The present 2D RANS-VOF model results are also in close correlation with those of Zou *et al.*(2008) using a recently developed 3D Navier–Stokes solver for unstructured tetrahedral grids,

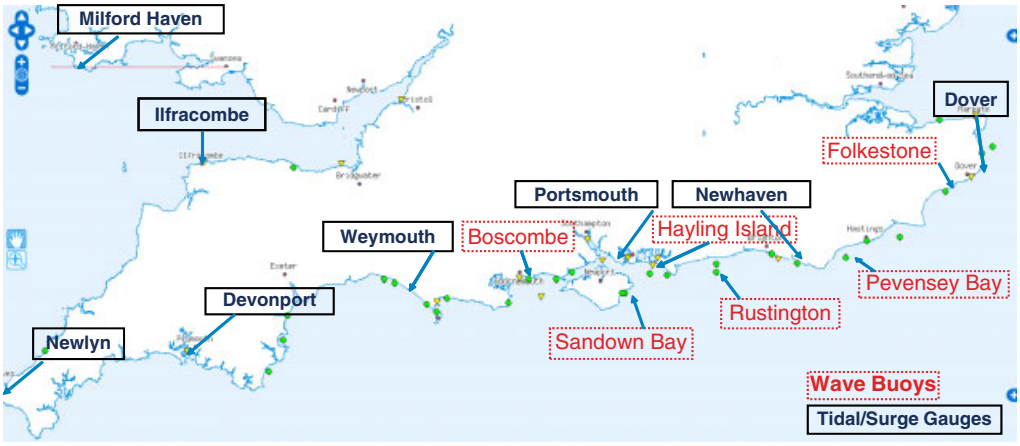


**Figure 8.** Location of tide/surge gauges and wave buoys for model calibration of wave, tide and surge model. This figure is available in colour online at wileyonlinelibrary.com/journal/qj

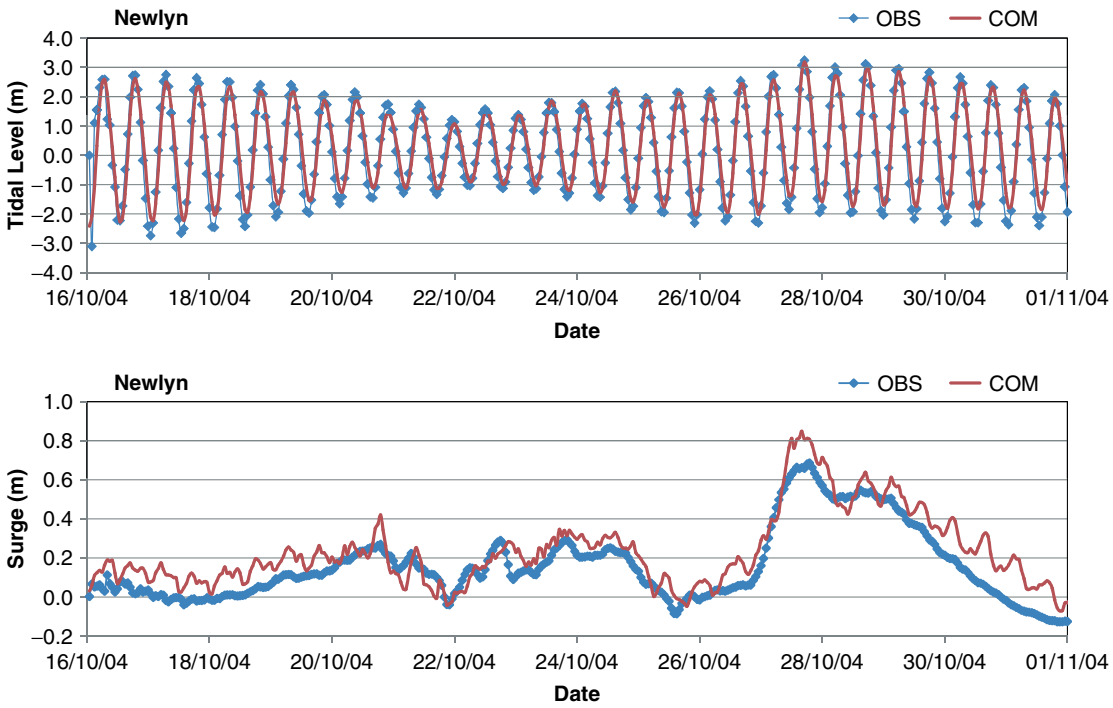


**Figure 9.** Comparison of computed tidal levels (top) and surge (bottom) from the control conditions (solid line) with measurements at Newlyn (dots). This figure is available in colour online at wileyonlinelibrary.com/journal/qj

with a novel hybrid level set/volume of fluid (LS/VOF) free surface capturing scheme (Lv *et al.*, 2010, 2012; Zou *et al.*, 2009).

## 5. Ensemble modelling results

### 5.1. *Meteorological modelling*

The wind direction and speed are averaged over a limited area at the entrance of the English Channel (indicated by the dashed box in Figure 3) at each hour for the 50 ensemble members, and is displayed in Figure 12. The atmospheric conditions over this area are likely those driving the surge and wave heights in the English Channel, such as those observed at the Newlyn site. Wind variables derived from the downscaled reanalysis data (WRF-ERA) are indicated as the 'control' case (red solid line). The ensemble mean forecast of wind speed generally outperforms the deterministic forecast at all lead times, while exhibiting a very small growth in ensemble divergence (Figure 12(b)). However, for wind direction (Figure 12(a)) a much greater divergence within the ensemble is evident, although the ensemble mean still appears to be more reliable than the deterministic forecast. The large divergence in the ensemble reflects differences in the storm track among members, with even a small geographic displacement of the low-pressure system resulting in a marked shift in the wind direction in the limited domain considered here.

### 5.2. *Wave, tide and surge modelling*

While differences in wind and sea surface pressure fields are key factors in producing different surge and wave heights, so too are the rate at which the storm develops and the track it takes. With in the 50 ensemble members a variety of storm tracks exist, with a sample shown in Figure 13

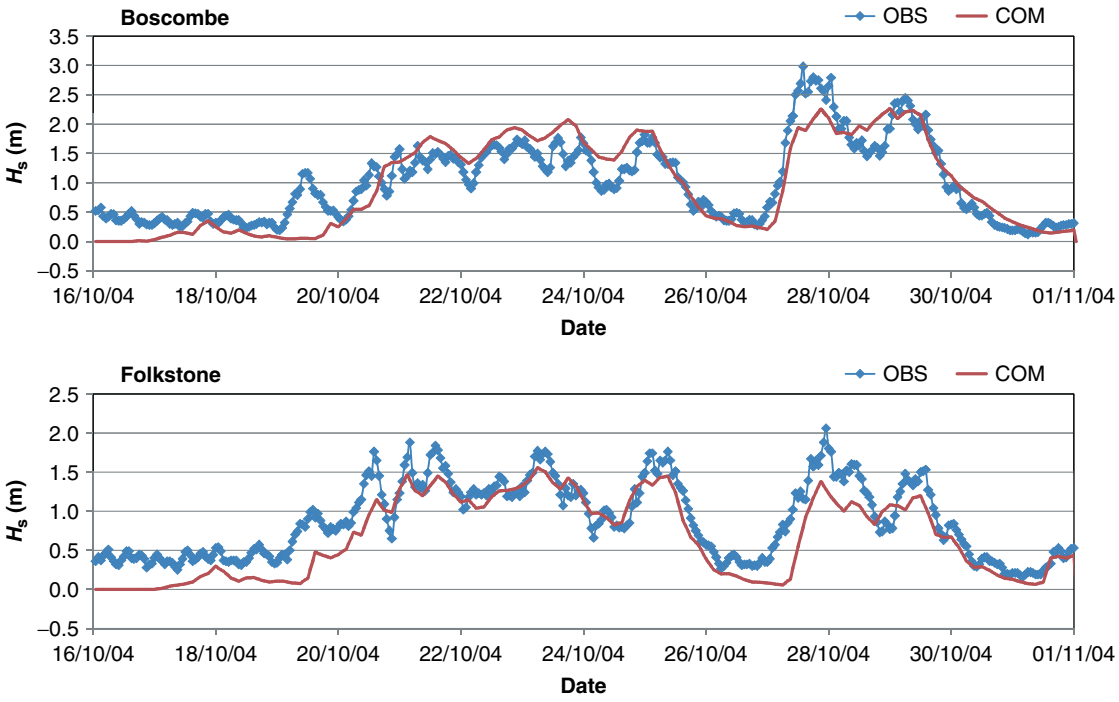


**Figure 10.** Comparison of computed wave heights from the control conditions (solid line) with the measurements at Boscombe and Folkstone (dots). This figure is available in colour online at wileyonlinelibrary.com/journal/qj

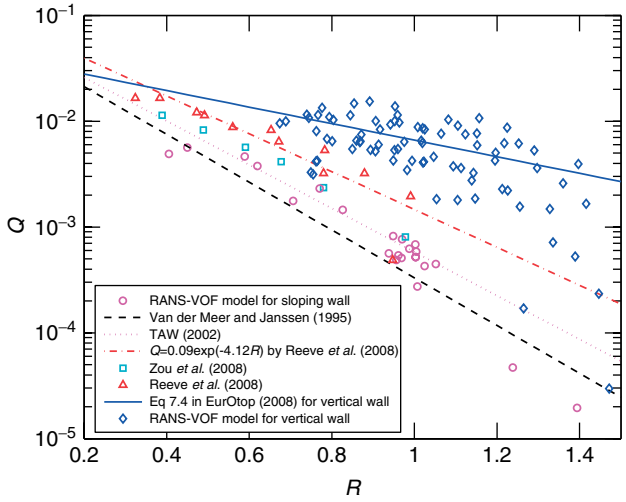


**Figure 11.** Comparisons of dimensionless overtopping discharge between numerical model and empirical formulae, $Q = q_{t0}/\sqrt{gH_s^3}$ against the relative freeboards, $R = R_c/H_s\xi_m$, where $\xi_m$ is surf similarity at the mean wave period at the toe of structures for a slope wall and is equal to one for a vertical wall (Peng and Zou, 2011, Figure 3). Diamond dots and solid line represent the wave overtopping over a vertical wall by the present RANS-VOF surf zone model and by the empirical formula, Equation 7.4 in the EurOtop manual (2008), respectively. This figure is available in colour online at wileyonlinelibrary.com/journal/qj

(ensemble members E06, E08, E39 and E46). To examine the uncertainty in wave, tide and surge modelling, 50 ensemble members from the meteorological model are used, together with the control conditions. It should be noted that the control conditions are derived from reanalysis data, which benefits from assimilation of a much greater number of observation data, whereas each member of the ensemble is an operational forecast. All ensemble members are generated from a particular initial date based on the control conditions on that date for a prescribed forecast duration. Here, three initial dates are used: 22, 24 and 26 October, The model was run for 10 days from each initial date, covering the storm peak (27–28 October). These cases are denoted as $T + 6$ day, $T + 4$ day and $T + 2$ day respectively. Due to the fact that the short-term weather changes have no influence on the tidal component of the total water-level elevation, this study focuses only on the results of ensemble predicted waves and surge.

First, the spatial variance of the computed wave heights was examined, particularly for the four selected ensemble members (E06, E08, E39, and E46) described previously. Although not shown here, the comparisons of the computed wave heights with initial dates of 22 October 2004 ($T + 6$ day) and 26 October 2004 ($T + 2$ day) clearly indicate that the variance of the predicted wave and surge results among the ensemble members from $T + 6$ day predictions is much larger than that from $T + 2$ day predictions, due to the wider spread of the storm tracks for $T + 6$ day than for $T + 2$ day, as shown in Figure 13. Therefore, the uncertainties of the wind and pressure fields generated from the meteorological model, represented by the ensemble members, have clearly propagated through to the predicted regional wave field.

Figure 14(a) illustrates the spatial distribution of the averaged significant wave heights ($H_s$) from 50 ensemble members over the downscaled fine-grid domain (indicated by the big box in Figure 4, right panel) covering the English Channel, at 0000 UTC 28 October 2004 for the initial date 26 October 2004 ($T + 2$ day). High waves around 7.5–8.0 m can be seen at the southwest of the English Channel, before gradually losing their strength as they propagate along the channel. Closer examination shows strong wave diffraction at the study site of Newlyn. Figure 14(b) shows the normalized standard deviation, defined as the ratio of standard deviation (STD) and averaged significant wave height ($H_s$), for the same area. In general, the normalized STD in the area is around 0.2–0.25, while the value appears to be larger in the areas where the waves are small. At the

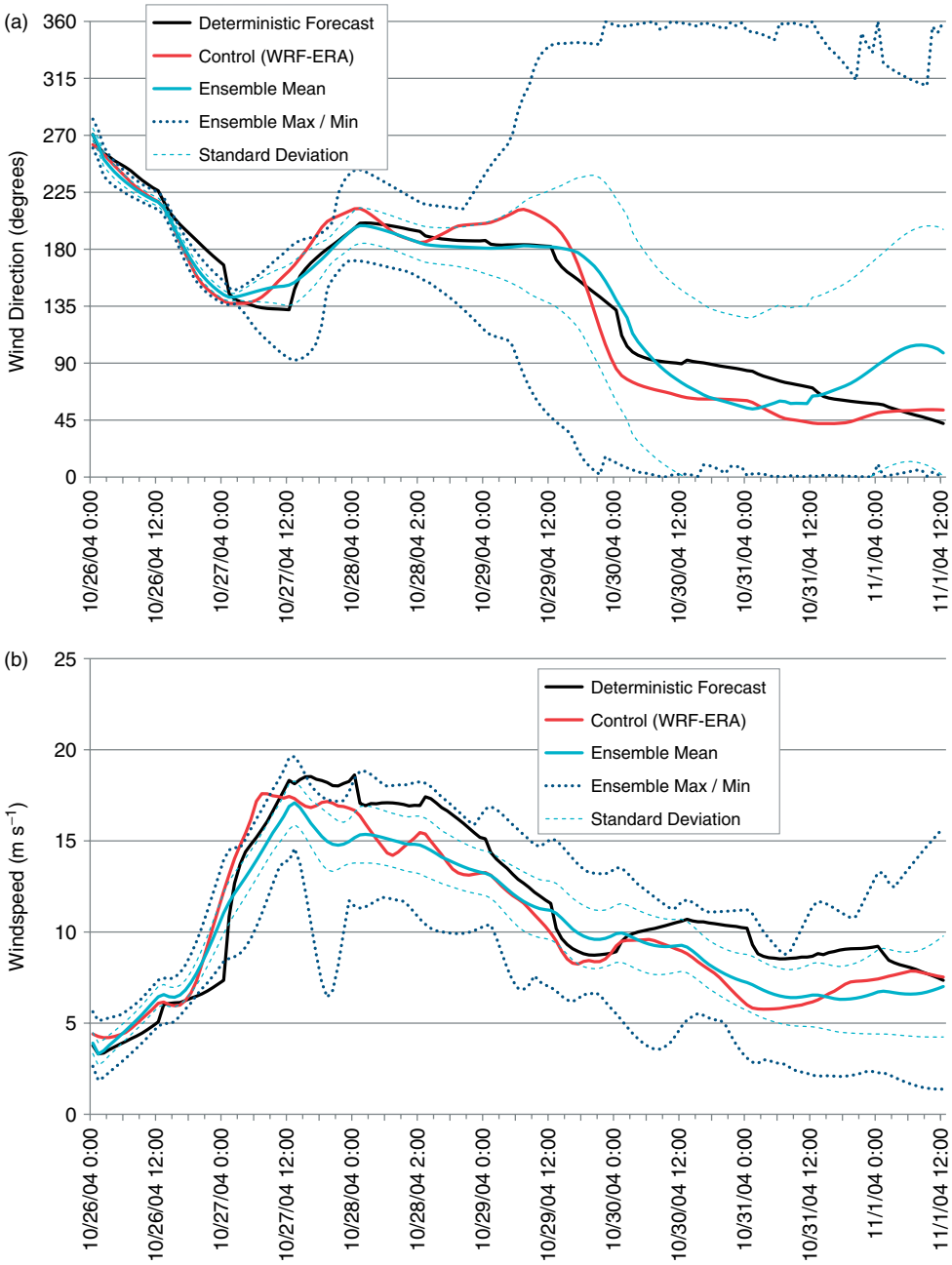


**Figure 12.** Mean wind direction (a) and speed (b) in the limited area domain at the western entrance to the English Channel (identified as dashed box in Figure 3). Horizontal axis is UTC time. This figure is available in colour online at wileyonlinelibrary.com/journal/qj

Newlyn site, this means a maximum absolute STD of wave height of ∼1.55 m at the storm peaks.

To illustrate the temporal variation of the predicted wave heights at selected locations, time series from all 50 ensemble members can be extracted and presented as a 'spaghetti diagram' (not shown here). The diagram shows the range of the predicted wave heights and hence the uncertainties in wave height predictions. The detailed time series results can also be used for a further statistical analysis, including the ensemble mean, maximum and minimum envelope and the standard deviation. Such measures can assist in quantifying the uncertainty cascading from the meteorological data to the hydrodynamics in the oceanic and coastal areas.

As an example, Figure 15 shows the computed wave heights at Boscombe, averaged from 50 ensemble members with the initial date 26 October 2004 ($T + 2$ day), denoted as 'Ensemble Mean'. Also shown in Figure 15 are the computed wave heights from the control condition (Control), the measured wave heights (Measurements), the maximum/minimum envelope (Ensemble Max/Min), as well as the standard deviation range (Standard Deviation).

### 5.3. *Nearshore wave modelling*

The 50 ensemble members of wave and water elevation generated by the POLCOMS/ProWAM models are used to drive the SWAN model. Figure 16 shows the evolution of the ensemble mean significant wave height and wave direction at water depths of 10 m, 18 m and 43 m predicted by SWAN (the yellow squares in Figure 5 denote the locations of SWAN outputs). Wave direction is defined according to nautical convention (i.e. the direction from which the wind or the waves come, measured clockwise from geographic north). Significant wave height decreases from the offshore deep

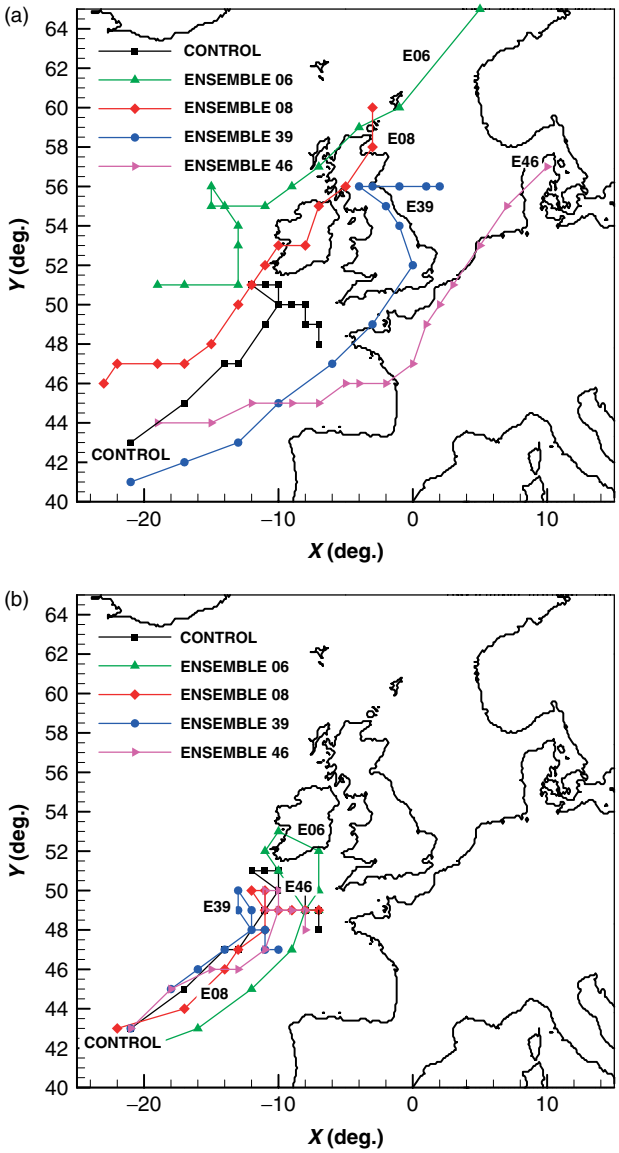


**Figure 13.** Storm tracks of four selected members of the ensemble and the control conditions at 6-hourly intervals between 1200 UTC 26 October 2004 and 0000 UTC 30 October 2004 for: (a) $T + 6$ day forecast (initial date: 22 October 2004); (b) $T + 2$ day forecast (initial date: 26 October 2004). This figure is available in colour online at wileyonlinelibrary.com/journal/qj

water to the shallower water depth due to wave refraction, wave breaking and bottom friction. The peak offshore wave height occurs around 0000 UTC 28 October, whereas the peak wave height in 10 m water depth occurs 6 hours earlier, when the water level becomes highest due to combined high tide and surge (Figure 9). As shown by the solid lines in Figure 16 (right panel), the offshore wave direction is southerly initially (at 0000 UTC 27 October wave direction is 180°), before changing to southeasterly as the storm approaches (wave direction <180°), and then southwesterly during and after the storm (wave direction >180°). This temporal evolution of wave direction correlates well with the wind direction variation predicted by the meteorological model shown in Figure 12(a). At shallower water depths of 10 and 18 m, the waves become perpendicular to the depth contours and coastlines, due to refraction. Tidal modulation of the wave direction is also apparent at these two locations (Figure 16, right panel).

The shadow zone in Figure 16 shows the standard deviations of the ensemble of wave height and wave direction. The left panel indicates that the normalized standard deviations of wave height increase from offshore to shallow water depth, while the wave height decreases towards shore due to enhanced breaking and bottom-induced dissipation. The standard deviation in wave height grows until the wave height reaches a maximum and remains nearly the same after that, which is consistent with the similar trend in wind speed in Figure 12(b). The standard deviation in wave direction becomes much greater and no longer reliable after 30 October, as a result of a similar trend of wind direction illustrated in Figure 12(a).

### 5.4. *Surf zone modelling*

The SWAN output of 50 ensemble members of significant wave height and period and the water elevations from the POLCOMS/ProWAM models at 10 m water depth are used to drive the 2DV RANS-VOF model simulation over the sloping beach indicated by the straight line over the squares in Figure 5. The RANS-VOF model determines the wave transformation due to shoaling, breaking and reflection, and the overtopping discharge at the sea wall. As an independent check, the same ensemble of offshore wave condition and water level are used to evaluate significant wave height $H_s$ and peak wave period $T_p$ at the toe of the structure using Goda's (2009) surf zone model, which in turn are used to drive the deterministic empirical overtopping formula to calculate the overtopping discharge (cf. Eq. 7.3 in the EurOtop Manual, 2008). We found that these two sets of results for $H_s$ and $T_p$ at the toe of the structure were in good agreement.

The RANS-VOF model was used to generate an ensemble of 50 realizations of overtopping discharge rate using the methods described in section 4.3. For each ensemble member, simulations were performed for the following times: 1600 UTC 27 October, 1700 UTC 27 October, 0400 UTC 28 October, 0500 UTC 28 October, 1700 UTC 28 October and 1800 UTC 28 October. Overtopping rates are largely determined by water level, in addition to wave conditions. Thus it was anticipated that overtopping reached its maximum at the combination of large waves and high water levels.

Figure 17 shows the significant wave height, tide and surge level, and the comparison of overtopping discharge predicted by the empirical formula and RANS-VOF surf zone model. There are large standard deviations at storm peaks and after 28 October, but small standard deviations during 27 October. The uncertainty in surges is negligible (middle panel). The ensemble mean of overtopping discharge (black circles bottom panel) is in good agreement with the control case (red solid line) at the peak of the storm, 6 hours before 0000 UTC 28 October 2004. The standard deviation of overtopping discharge is large at the storm peaks, but the control case is located inside one standard deviation around the ensemble mean (dashed-dotted lines, bottom panel). Overtopping discharge computed with the RANS-VOF surf zone model (circles) has large uncertainty (black bars). However, Figure 17 (bottom panel) shows that the ensemble mean of overtopping predicted by the RANS-VOF model (black circles) is in good agreement with that calculated by Goda's (2009) surf zone model, together with the empirical overtopping formulae of EurOtop

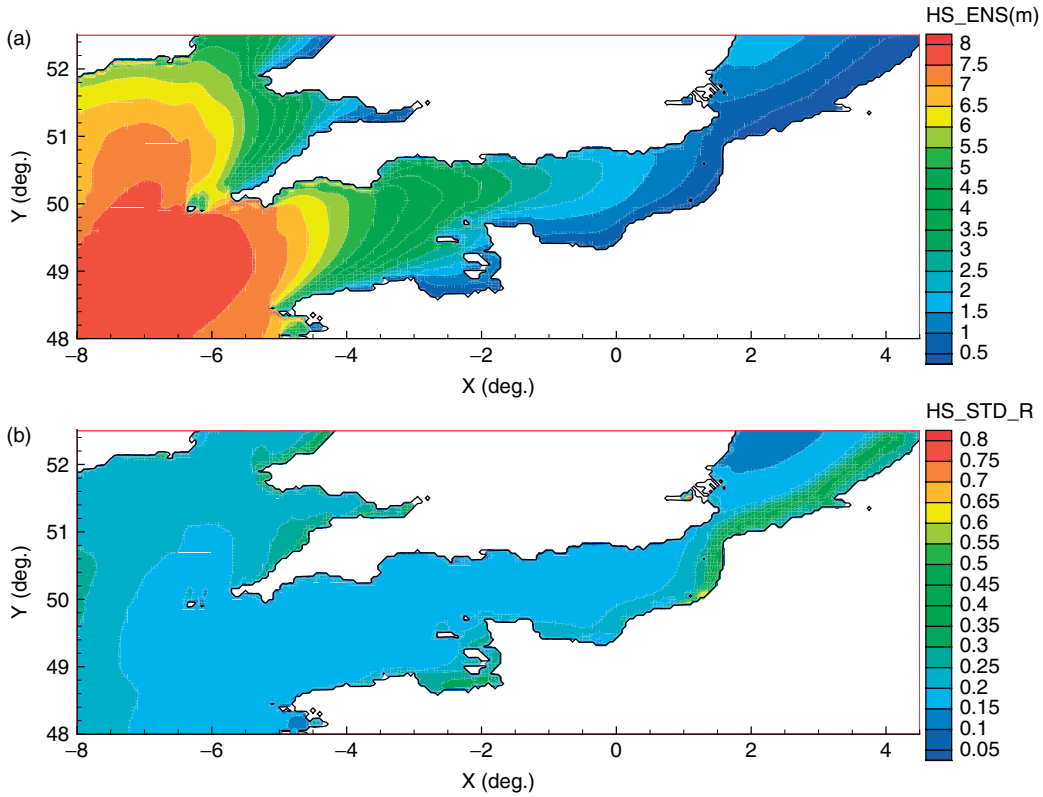


**Figure 14.** $T + 2$ day forecast (initial date: 26 October 2004): (a) ensemble average significant wave height ($H_s$); (b) normalized standard deviation (STD/$H_s$) at 0000 UTC 28 October 2004. This figure is available in colour online at wileyonlinelibrary.com/journal/qj

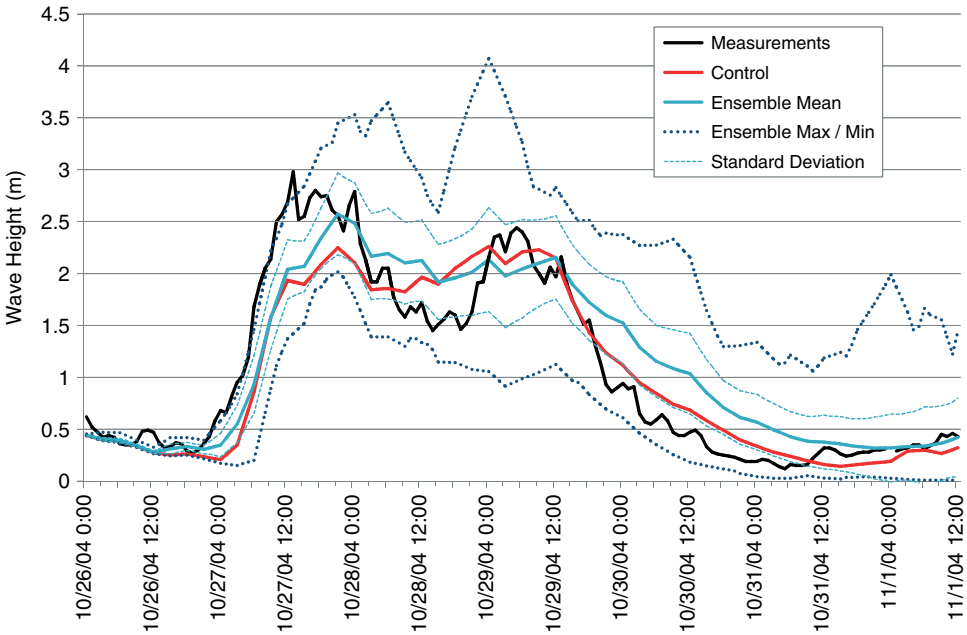


**Figure 15.** Statistical analysis of the computed and observed significant wave heights at Boscombe (initial date 26 October 2004). Horizontal axis is UTC time. This figure is available in colour online at wileyonlinelibrary.com/journal/qj

(2008) (solid lines). Nonetheless, the standard deviation of overtopping discharge predicted by RANS-VOF (black error bars) varies between 60% to 100% of the ensemble mean value and is substantially larger than that predicted by the empirical overtopping formula (dashed-dotted lines). The standard deviation of overtopping discharge predicted by RANS-VOF (black bars) is due to modelling error, randomness and turbulent nature of overtopping, as well as the standard deviation in wave height of 50 ensembles at 10 m water depth predicted by the SWAN model. In contrast, the standard deviation of Goda+empirical overtopping formula (dashed-dotted line, bottom panel) comes solely from the standard deviation of wave height at the toe of the structure which is used to drive the deterministic empirical model to predict the overtopping rate. Using MIKE 21 spectral wave model and overtopping empirical formula to obtain the deterministic model prediction of overtopping at Newlyn sea wall, Magar *et al.* (2009) found mean and peak discharges

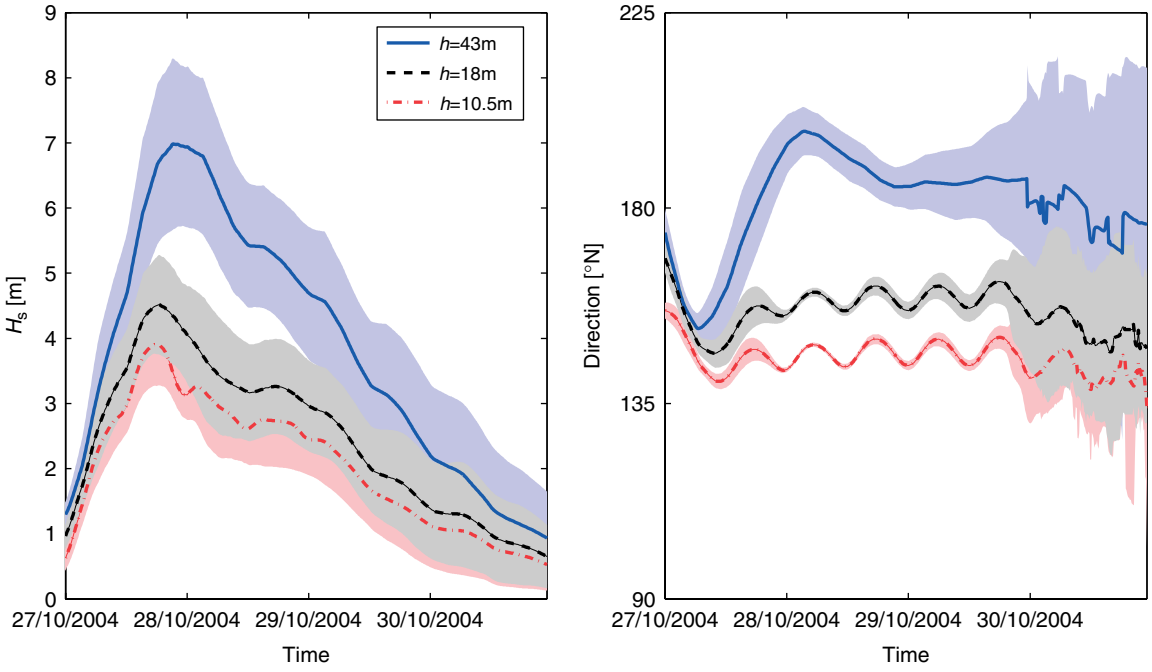


**Figure 16.** Ensemble mean of predicted wave height and direction by SWAN model at 43 m, 18 m and 10.5 m water depth at Newlyn Harbour (shadowed area indicates one standard deviation about the ensemble mean denoted by lines of same colour; the locations of the model output are indicated by the yellow squares in Figure 5). Horizontal axis is UTC time. This figure is available in colour online at wileyonlinelibrary.com/journal/qj

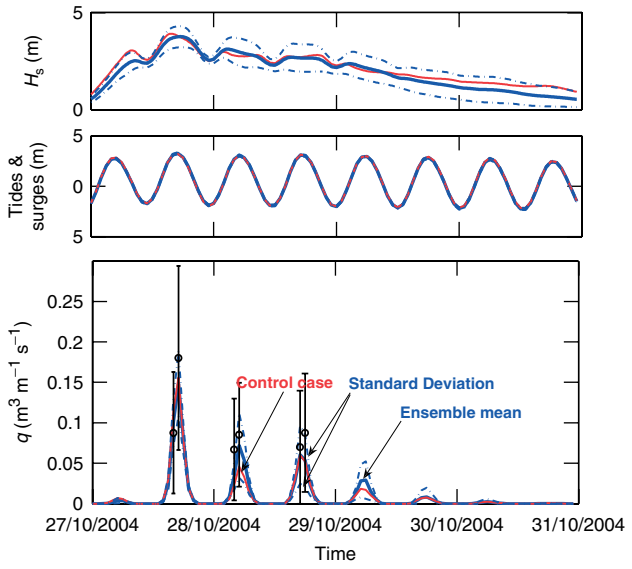


**Figure 17.** Top: significant wave height at 10.5 m water depth, ensemble mean (blue solid lines), control (red solid lines), standard deviation (dashed-dotted lines). Middle: tides and surges. Bottom; the predicted overtopping discharge, ensemble mean (black circles) and standard deviation (black error bars) of the RANS-VOF surf zone model results, predictions by empirical formulae in EurOtop manual (2008) (ensemble mean: blue solid lines; control: red solid line; standard deviation: blue dashed-dotted lines). Horizontal axis is UTC time. This figure is available in colour online at wileyonlinelibrary.com/journal/qj

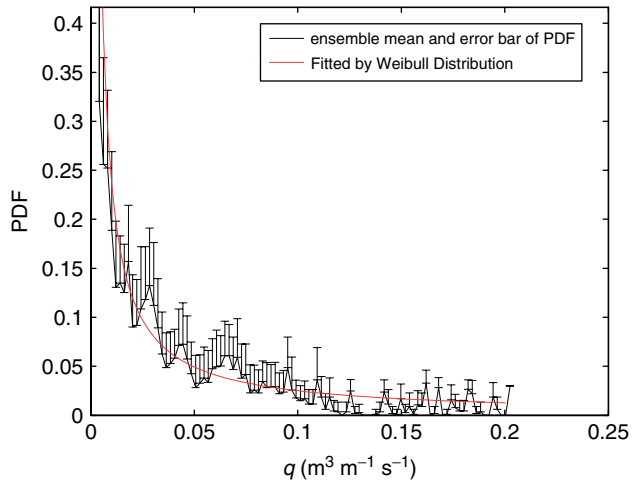


**Figure 18.** Probability distribution function of overtopping discharge at the damaged sea wall in Newlyn for the storm event between 27 October and 31 October 2004. This figure is available in colour online at wileyonlinelibrary.com/journal/qj

at Newlyn site to be between 10 and 100 L s$^{-1}$ m$^{-1}$. This is in general agreement with the present ensemble mean prediction in Figure 17 (bottom panel).

Figure 18 shows the probability distribution of the overtopping discharges for 50 ensemble members at 120 evenly distributed time instants between 27 and 31 October. Results show that the overtopping discharges are in the range 0–0.2 m$^3$ m$^{-1}$ s$^{-1}$. The smooth solid red line represents the ensemble mean of probability distribution of overtopping discharge among 50 ensemble members, while the black error bars represent the standard deviation around the ensemble mean values (black solid line attached to error bars). The best-fit Weibull distribution for these data is given by $0.0052q^{-0.92}\ \exp(-0.065q^{0.08})$. Figure 18 gives the likelihood for different overtopping events occurring between 27 and 31 October and the uncertainty associated with the prediction.

Figure 18 also suggests that about 50% of the overtopping events exceed 0.05 m$^3$ m$^{-1}$ s$^{-1}$, which is the damage threshold for revetment sea walls (see EurOtop, 2008). That is, the ensemble modelling gives a strong indication that damage would occur. Both the predicted overtopping and damage were observed in the real world, as shown in

Figure 1. How much damage and its nature, however, are not predicted by the threshold approach.

## 6. Discussion

Meteorological model results from the dynamical downscaling of reanalysis data with the WRF model for a case study of an extreme UK storm event (25–30 October 2004) are presented here. More accurate representations of the surface wind and atmospheric pressure fields are found in downscaled data compared with ERA-Interim data. A further benefit stems from improved wave and surge predictions using the high temporal and spatial resolution WRF output.

The ECMWF Ensemble Prediction System (EPS) is used to generate a 50-member perturbed physics ensemble with a forecast initial time of 0000 UTC 26 October 2004 ($T + 2$ day forecast). Sixty hours into the forecast, just past the storm peak, the differences in the intensities of the storm between ensemble members become significant. Differences in the storm track and translation speed between ensemble members result in large deviations in predicted wave heights (Figures 14 and 15). Through comparisons with observed storm wave heights and surge levels we found that greater confidence may be placed in the $T + 2$ day predictions than $T + 4$ day predictions (Chen *et al.*, 2010). More importantly, the ensemble mean results are in better agreement with observations than those predicted with the deterministic forecast, which is consistent with the findings of Horsburgh *et al.*(2008) and Flowerdew *et al.*(2010).

The accuracy of the forecast of storm-induced ocean waves by ProWAM and SWAN is largely dependent on the quality of wind data. For the individual storm in the open ocean, uncertainty in the wind field propagates into wave height uncertainty, and may be doubled since the dimensionless wave height is approximately proportional to the square of the wind speed. As shown in Figures 12 and Figure 14(b), the normalized standard deviation (standard deviation/mean), increases from 8% in modelled wind speed to 20–25% in wave height in the English Channel.

The wind–wave relationship is much more complicated in the coastal region since waves are further affected by distance offshore, coastal sheltering, fetch-limited wave growth, nonlinear wave–wave interaction, bathymetric and other local effects, which would introduce further uncertainty into wave height predictions.

After waves enter Newlyn Harbour at an intermediate water depth of about 50 m, the wave height decreases and the normalized standard deviation of wave height increases towards the shore from about 17% at 43 m water depth to about 25% at 18 m (Figure 16). A similar trend is visible in Figure 14(b) for other coastal bay areas. This is possibly due to coastal sheltering, limited fetch and local bathymetric change. The normalized standard deviation of wave direction, however, decreases drastically to almost zero towards the shore. The reason for this behaviour is two fold: (i) the wave directions become perpendicular to depth contour near the shoreline due to wave refraction; (ii) only waves from certain directions are allowed to enter Newlyn Harbour. Most wave directions have limited fetch in the English Channel. At the entrance of Newlyn Harbour, the fetch for the south and southwest directions is almost unlimited from North Atlantic storms. The uncertainty propagation through the wave height and direction in the nearshore region is found to be site specific (see Figure 14(b)).

Our study indicates that the predicted magnitude, time and location of maximum overtopping discharge can deviate drastically among ensemble members. The standard deviation of overtopping discharge varies between 60% and 100% of the ensemble mean value (Figure 17), which is about three to five times that of the incident wave height. These results indicate the importance of including the uncertainty estimate in the overtopping and flooding prediction. As shown in Figure 11, the overtopping is proportional to ${H_s}^{3/2}$ and decreases exponentially with increasing relative freeboard ($R_c/H_s$) according to the overtopping empirical model. The randomness of the incoming waves and the nonlinear and turbulent nature of wave–structure interaction further contribute to the uncertainty in the overtopping predictions by the RANS-VOF surf zone model.

For this particular event, the forward speed of the storm in more than 70% of the ensemble members exceeds the 20 m $s^{-1}$ threshold identified by Lennon (1964) as a key to producing a significant surge event. In addition, as shown by Xu *et al.*(2007) and Zhang and Perrie (2008), wave heights and wavelength increase with storm translation speed, reaching their maxima when the wave energy propagation speed is about the same as the translation speed. The peak of wave height lags behind that of wind speed (Figures 12 and 16), partly because the translation speed of the storm exceeds the wave energy propagation speed.

## 7. Conclusions

In this study, we integrate meteorological models, regional hydrodynamic (waves, tides and surge) models, and surf zone hydrodynamic models to construct an ensemble prediction framework of coastal flood risk due to overtopping at sea defences. Despite the uncertainties in each interlinked model, and the uncertainty propagation from meteorological model to coastal and surf zone models, the outputs of the interlinked ensemble modelling framework are in accord with the reality of the flooding and sea wall damage events observed. In addition, the uncertainties do not appear to be compounded to the extent that the ensemble mean is no longer a useful measure. The ensemble mean is in closer agreement with the observation than the control case (Figure 15).

The downscaled, high-resolution meteorological data yield better predictions of surface wind and atmospheric pressure fields, and thus improved wave and surge predictions. The differences in the storm intensities, storm tracks and translation speed results in large deviations in predicted wave heights but relatively small deviation in surge.

Within the model framework, the uncertainty has been shown to more than double while propagating from the wind field forecast to wave height prediction. This result is a physically consistent feature given that the dimensionless wave height is approximately proportional to the square of wind speed in the open ocean. However, the uncertainty is reduced while propagating from the sea-surface pressure to the surge, mainly due to the water depth change and fetch limit.

Although the propagation of uncertainty in wave from open ocean to the coast is site dependent, since wave transformation is subject to local effects in the coastal region,

the trend should be similar at other sites. After waves enter Newlyn Harbour, the normalized standard deviation of wave height increases towards the shore. However, the normalized standard deviation of wave direction decreases drastically to almost zero towards the shore due to wave refraction and coastal sheltering.

Large uncertainty exists in the magnitude, time and location of maximum overtopping discharge. The standard deviation of overtopping discharge is three to five times that of incident wave height (Figure 17). Therefore, it is important to include the uncertainty estimate in the overtopping and flooding prediction.

Since the high tide at Newlyn is four to five times greater than the peak storm surge, tidal modulation of wave magnitude and direction is dominant over surge for this storm (Figures 9 and 16). Thus uncertainty in storm surge has a negligible effect on the overtopping predictions. Maximum overtopping and flooding occur before the storm peak, at high tide and surge, indicating the importance of accurate water-level and bed-level predictions.

Future climate change will very likely impact the intensity and frequency of extratropical cyclones over Europe (IPCC, 2007). The October 2004 storm discussed here was a significant event for the southern region of the UK. It has been postulated that the return period for extreme wind speeds may be reduced in future climates (Leckebusch *et al.*, 2006; Pinto *et al.*, 2007; Ulbrich *et al.*, 2009), making this type of event more likely to occur. Coastal flood defences in the UK have typically been designed to withstand storm events with a return period of 50–100 years, and may therefore be inadequate in the future as the magnitude of storms with this return period increases. The 'Clouds-to-Coast' approach developed in this study is generic and can be utilized to estimate the flood and damage at other sites and/or for potential future storms.

## Acknowledgement

The authors would like to thank Drs Xin Lv, Adrián Pedrozo-Acuña, Judith Wolf, Dawei Han, Miguel Rico-Ramirez, and Zhengyi Wang for their contributions at the early stage of this project. This research was supported by the Flood Risk from Extreme Events (FREE) Programme of the UK Natural Environment Research Council (NERC) (NE/E0002129/1), coordinated and monitored by Professors Chris Collier and Paul Hardaker. During the course of this project, we have benefited from discussing with our partners, Proudman Oceanographic Laboratory, the Channel Coastal Observatory (and New Forest District Council), Halcrow Group Ltd. The first author would also like to acknowledge the support of the start-up fund provided by the University of Maine at Orono during the late stage of this project.

## References

Booij N, Ris RC, Holthuijsen LH. 1999. A third generation wave model for coastal regions. Part I. Model description and validation. *J. Geophys. Res.* **104**(C4): 7649–7666.

Chen F, Dudhia J. 2001. Coupling an advanced land-surface/hydrology model with the Penn State/NCAR MM5 modeling system. Part I. Model description and implementation. *Mon. Weather Rev.* **129**: 569–585.

Chen Y, Pan S, Hewston R, Cluckie I. 2010. 'Ensemble modelling of tides, surge and waves'. In *Proceedings of the 20th International Offshore (Ocean) and Polar Engineering Conference*, CD-ROM.

CIRIA. 1986. 'Sea walls: survey of performance and design practice'. CIRIA Technical Note 125, London.

CIRIA & CUR. 1991. *Manual on the Use of Rock in Coastal and Shoreline Engineering*, CIRIA Special Publication 83/CUR Report 154, London.

Dance SL, Zou QP. 2010. HESS opinions: 'Ensembles, uncertainty and flood prediction'. *Hydrol. Earth. Syst. Sci. Discuss.* **7**: 3591–3611.

DEFRA. 2005. Making space for water: taking forward a new Government strategy for flood and coastal erosion risk management in England. First Government response to the autumn 2004 Making space for water consultation exercise. http://archive.defra.gov.uk/environment/flooding/documents/policy/strategy/strategy-response1.pdf

Dudhia J. 1989. Numerical study of convection observed during the winter monsoon experiment using a mesoscale two-dimensional model. *J. Atmos. Sci.* **46**: 3077–3107.

EurOtop. 2008. *Wave Overtopping of Sea Defences and Related Structures: Assessment Manual*, Pullen T, Allsop NWH, Bruce T, Kortenhaus A, Schuttrumpf H, Van der Meer J (eds). www.overtopping-manual.com

Flather RA. 1984. A numerical model investigation of the storm surge of 31 January and 1 February 1953 in the North Sea. *Q. J. R. Meteorol. Soc.* **110**: 591–612.

Flather RA, Williams JA. 2004. 'Future development of operational storm surge and sea level prediction'. Proudman Oceanographic Laboratory, Internal Document No. 165.

Flowerdew J, Horsburgh K, Wilson C, Mylne K. 2010. Development and evaluation of an ensemble forecasting system for coastal storm surges. *Q. J. R. Meteorol. Soc.* **136**: 1444–1456.

Garcia N, Lara JL, Losada IJ. 2004. 2-D numerical analysis of near-field flow at low-crested permeable breakwaters. *Coastal Eng.* **51**: 991–1020.

Goda Y. 2009. A performance test of nearshore wave height prediction with CLASH datasets. *Coastal Eng.* **56**: 220–229.

Günther H, Hasselmann S, Janssen PAEM. 1992. 'The WAM model Cycle 4 (revised version)', German Climate Centre: Hamburg, Technical Report No. 4.

Hirt CW, Nichols BD. 1981. Volume of fluid (VOF) method for the dynamics of free boundaries. *J. Comput. Phys.* **39**: 201–225.

Holt JT, James DJ. 2001. An s-coordinate density evolving model of the northwest European continental shelf: 1, Model description and density structure. *J. Geophys. Res.* **106**: 14015–14034.

Hong S-Y, Dudhia J, Chen S-H. 2004. A revised approach to ice microphysical processes for the bulk parameterization of clouds and precipitation. *Mon. Weather Rev.* **132**: 103–120.

Hong S-Y, Noh Y, Dudhia J. 2006. A new vertical diffusion package with an explicit treatment of entrainment processes. *Mon. Weather Rev.* **134**: 2318–2341.

Horsburgh KJ, Williams JA, Flowerdew J, Mylne K. 2008. Aspects of operational forecast model skill during an extreme storm surge event. *J. Flood Risk Manage.* **1**: 213–221.

Hunt-Raby A, Borthwick AGL, Stansby PK, Taylor PH. 2011. Experimental measurement of focused wave group and solitary wave overtopping. *Journal Hydraul. Res.* (Special Issue) **49**: 450–464.

IPCC. 2007. 'Impacts, Adaptation and Vulnerability'. In *Working Group II to the Fourth Assessment Report of the Intergovernmental Panel on Climate Change*, Parry ML, Canziani OF, Palutikof JP, Van der Linden PJ, Hanson CE (eds), Cambridge, UK.

Kain JS. 2004. The Kain–Fritsch convective parameterization: an update. *J. Appl. Meteorol.* **43**: 170–181.

Lara JL, Garcia N, Losada IJ. 2006. RANS modelling applied to random wave interaction with submerged permeable structures. *Coastal Eng.* **53**: 395–417.

Leckebusch GC, Koffi B, Ulbrich U, Pinto JG, Spangehl T, Zacharias S. 2006. Analysis of frequency and intensity of European winter storm events from a multi-model perspective, at synoptic and regional scales. *Climate Res.* **31**: 59–74.

Lennon GW. 1964. The identification of weather conditions associated with the generation of major storm surges along the west coast of the British Isles. *Q. J. R. Meteorol. Soc.* **90**: 495–497.

Lin PZ, Liu PLF. 1998. A numerical study of breaking waves in the surf zone. *J. Fluid Mech.* **359**: 239–264.

Losada IJ, Lara JL, Guanche R, Gonzalez-Ondina JM. 2008. Numerical analysis of wave overtopping of rubble mound breakwaters. *Coastal Eng.* **55**: 47–62.

Lv X, Zou Q-P, Zhao Y, Reeve DE. 2010. A novel coupled level set and volume of fluid method for sharp interface capturing on 3D tetrahedral grids. *J. Comput. Phys.* **229**: 2573–2604.

Lv X, Zou Q-P, Reeve DE, Zhao Y. 2012. A preconditioned implicit free-surface capture scheme for large density ratio on tetrahedral grids, *Commun. Comput. Phys.* **11**: 215–248.

Magar V, Evans P, Jones O, William NWH. 2009. Damage from waves, surges and overtopping at vertical seawalls. In *Coasts, Marine Structures and Breakwaters 2009*. Institution of Civil Engineers: Edinburgh.

McCabe M, Stansby PK, Apsley DD. 2011. Coupled wave action and shallow water modelling for random wave run-up on a slope. *J. Hydraul. Res.* **49**: 515–522.
Meadowcroft IC, Reeve DE, Allsop NWH, Diment RP, Cross J. 1996. Development of new risk assessment procedures for coastal structures. In *Advances in Coastal Structures and Breakwaters*, Clifford JE (ed.). Thomas Telford: Slough, UK; 6–46.
Mlawer EJ, Taubman SJ, Brown PD, Iacono MJ, Clough SA. 1997. Radiative transfer for inhomogeneous atmosphere: RRTM, a validated correlated-k model for the longwave. *J. Geophys. Res.* **102**(D14): 16663–16682.
Monbaliu J, Padilla-Hernández R, Hargreaves JC, Carretero-Albiach JC, Luo W, Sclavo M, Günther H. 2000. The spectral wave model WAM adapted for applications with high spatial resolution. *Coast. Eng.* **41**: 41–62.
Office of Science and Technology (OST). 2004. *Foresight. Future Flooding. Scientific Summary*. Office of Science and Technology: London.
Osuna P, Wolf J, Ashworth M. 2004. 'Implementation of a wave-current interaction module for the POLCOMS system'. Internal Document No. 168, Proudman Oceanographic Laboratory, Liverpool, UK.
Pan S, Chen Y, Wolf J, Du Y. 2009. Modelling of waves in the Irish Sea: effects of oceanic wave and wind forcings. *Ocean Dynam.* **59**: 827–836.
Peng Z, Zou Q-P. 2011. Spatial distribution of wave overtopping water behind coastal structures. *Coastal Eng.* **58**: 489–498.
Persson A, Grazzini F. 2007. User guide to ECMWF forecast products. *ECMWF Meteorol. Bull.* M3.2.
Pinto JG, Zacharias S, Fink AH, Leckebusch GC, Ulbrich U. 2007. Changes in storm track and cyclone activity in three SRES ensemble experiments with ECHAM5/MPI-OM1 GCM. *Climate Dynam.* **29**: 195–210.
Pryor SC, Schoof JT, Barthelmie RJ. 2005. Climate change impacts on wind speeds and wind energy density in northern Europe: empirical downscaling of multiple AOGCMs. *Climate Res.* **29**: 183–198.
Reeve DE. 1998. On coastal flood risk. *ASCE J. Waterway Port Coastal Ocean Eng.* **124**: 219–228.
Reeve DE, Burgess KA. 1993. Assessment of coastal flood risk in England and Wales. *IMA J. Math. Appl. Business Ind.* **5**: 197–209.
Reeve DE, Soliman A, Lin PZ. 2008. Numerical study of combined overflow and wave overtopping over a smooth impermeable seawall. *Coastal Eng.* **55**: 155–166.
Schwierz C, Köllner-Heck P, Mutter EZ, Bresch DN, Vidale P-L, Wild M, Schär C. 2010. Modelling European winter wind storm losses in current and future climate. *Clim. Change* **101**: 485–514.
Schüttrumpf H, Oumeraci H. 2005. Layer thicknesses and velocities of wave overtopping flow at seadikes. *Coastal Eng.* **52**: 473–495.
Skamarock WC, Klemp JB, Dudhia J, Gill DO, Barker DM, Duda MG, Huang X-Y, Wang W, Powers JG. 2008. 'A description of the Advanced Research WRF version 3'. NCAR Technical Note NCAR/TN475+STR.
Shao S, Ji C, Graham DI, Reeve DE, James PW, Chadwick AJ. 2006. Simulation of wave overtopping by an incompressible SPH model. *Coast. Eng.* **53**: 723–735.
TAW. 2002. *Technical Report on Wave run-up and Wave Overtopping at Dikes*, van der Meer JW (ed.). Technical Advisory Committee for Flood Defence: Netherlands.
Tsuruta S, Goda Y. 1968. 'Expected discharge of irregular wave overtopping'. In *Proceedings of the 11th Conference on Coastal Engineering*, London. ASCE: New York; 833–852.
UK Met Office. 2010. Met Office Integrated Data Archive System (MIDAS) Land and Marine Surface Stations Data. http://badc.nerc.ac.uk/data/ukmo-midas. [Accessed on 16 December 2010].
Ulbrich U, Leckebusch G, Pinto J. 2009. Extra-tropical cyclones in the present and future climate: a review. *Theor. Appl. Climatol.* **96**: 117–131.
Van der Meer J, Janssen JPFM. 1995. Wave run-up and wave overtopping at dikes. In *Wave forces on inclined and vertical structures*, Kobayashi N, Demirbilek Z. (eds.) *ASCE*; 1–27.
Weisse R, von Storch H, Feser F. 2005. Northeast Atlantic and North Sea storminess as simulated by a regional climate model 1958–2001 and comparison with observations. *J. Climate* **18**: 465–479.
Williams JA, Flather RA. 2004. 'The Operational Storm Surge Model: maintenance, performance and development', January 2003–March 2004. Internal Document No. 164, Proudman Oceanographic Laboratory, Liverpool, UK.
Winter C, Chiou MD, Kao CC, Lee BC. 2008. 'Dynamic downscaling of meteorological fields for the hydrodynamic simulation of extreme events'. In *Proceedings of Coastal Engineering*.
Wolf J, Wakelin SL, Holt JT. 2002. 'A coupled model of waves and currents in the Irish Sea'. In *Proceedings of the 12th International Offshore and Polar Engineering Conference*, Vol. 3, Kitakyushu, Japan; 108–114.
Xu F, Perrie W, Toulany B, Smith PC. 2007. Wind-generated waves in Hurricane Juan. *Ocean Modelling* **16**: 188–208.
Zhang W, Perrie W. 2008. The influence of air–sea roughness, sea spray, and storm translation speed on waves in North Atlantic storms. *J. Phys. Oceanogr.* **38**: 817–839.
Zou Q-P, Peng Z. 2011. Evolution of wave shape over a low-crested structure. *Coastal Eng.* **58**: 478–488.
Zou Q-P, Reeve DE. 2009. Modelling water from clouds to coast. *Planet Earth*, Natural Environment Research Council, August issue, 22–23. http://planetearth.nerc.ac.uk/features/story.aspx?id=524
Zou Q-P, Reeve DE, Cluckie ID, Han D, Pan S, Rico-Ramirez MA, Wang Z, Lv X, Pedrozo-Acuña A, Chen Y. 2008. 'Ensemble prediction of inundation risk and uncertainty arising from scour (EPIRUS): an overview'. In *Proceedings of Floodrisk 2008*, 30 September–2 October 2008, Oxford, UK.
Zou Q-P, Reeve DE, Cluckie ID, Han D, Pan S, Wang Z, Lv X, Chen Y. 2009. 'Ensemble prediction of inundation risk and uncertainty arising from scour (EPIRUS)'. In *Proceedings of the 31st International Conference on Coastal Engineering*, Vol. 5; 4390–4400.

 